Waves of new results

Windmills in the ocean

AM2050B: Modelling 2B

F van der Top, S Williams,
S Deuten, T van der Valk

Delft University of Technology

TU Delft

Waves of new results

Windmills in the ocean

by

F van der Top, S Williams,
S Deuten, T van der Valk

Student Name	Student Number
F van der Top	5547105
S Williams	5549602
S Deuten	5600243
T van der Valk	5606667

Instructor: H Schuttelaar
Project Duration: April, 2023 - June, 2023
Faculty: Faculty of electrical engineering, mathematics and computer science, Delft

Style: TU Delft Report Style

TU Delft

Preface

Renewable energy is increasingly important to slow down climate change. Windmills are a great source for this energy production. As windmills take up a lot of land, building them in the ocean is a great solution to reduce the space they take in. Unfortunately, this does not come without problems. This report attempts to investigate the effects of the waves and seismic activities on a windmill placed in the ocean, and to investigate if the frequencies of both the windmill and the sources of the forces can cause resonance, as this has a big impact on the durability of a windmill.

F van der Top, S Williams,
S Deuten, T van der Valk
Delft, July 2023

Contents

List of Figures

Nomenclature

Overview of abbreviations and symbols used in this paper.

Abbreviations

Abbreviation	Definition
BCs	Boundary Conditions
ICs	Initial Conditions
ODE	Ordinary Differential Equation
PDE	Partial Differential Equation
HEM	Horizontal Earthquake Model

Variables

Symbol	Definition	Unit
x	Vertical position	$[m]$
t	Time	$[s]$
$u(x,t)$	Deflection of the beam	$[m]$
$F(x,t)$	Forcing Term	$[N]$
$v(x,t)$	Horizontal wave velocity	$[m/s]$

Constants for model

Symbol	Definition	Formula	Value	Unit
L	Length of beam		150	$[m]$
H	Length of beam in water		50	$[m]$
E	Elastic modulus		$210 \cdot 10^9$	$[Pa]$
I	Second moment of area	$\frac{\pi}{4}({R_2}^4 - {R_1}^4)$	1.73	$[m^4]$
V	Volume per unit length	$\pi {R_2}^2$	15.9043	$[m^2]$
A	Area beam profile	$\pi {R_2}^2 - \pi {R_1}^2$	0.6990	$[m^2]$
C_a	Added mass coefficient	$\frac{\rho_{steel}}{\rho_{sea}}\left(1 - \left(\frac{R_1}{R_2}\right)^2\right)$	0.33496	
C_d	Drag coefficient		1.17	
R_1	Inner radius		2.2	$[m]$
R_2	Outer radius		2.25	$[m]$
T	Wave period		5.7	$[s]$
a	Wave amplitude		1.5	$[m]$
k	Wavenumber	$2\pi/\lambda$	0.186	$[m^{-1}]$
ρ_{sea}	Sea water density		1030	$[kg/m^3]$
ρ_{steel}	Steel density		7850	$[kg/m^3]$
μ	Mass per unit length	$A\rho_{steel}$	5487	$[kg/m]$
σ	Wave frequency	$2\pi/T$	1.1023	$[s^{-1}]$
λ	Wavelength		33.8	$[m]$

1 Introduction

As tides change, so does humanities need for electricity. For many years these needs were met using greenhouse emitting processes. In recent years electricity provided by windmills has become an essential form of renewable energy. As of 2022, 7.5% of the global energy production is attributed to windmills, [4].

With more space being taken up by windmills on land, and pressure to not overbuild close to densely populated areas, sea wind farms are to be explored. To this end, more hazardous locations are to be used for wind farm construction. This can include areas prone to seismic shocks. Literature regarding stability of windmills in regions with seismic activity focuses on the interaction of the windmill and the sea bottom, and the base of the windmill. For more details the reader is advised to review [3]. The rigidity of the windmill is not the focus the literature. Therefore the relation between the rigidity of the windmill and the effect of seismic and water waves on deflection of the windmill is to be studied. This leads to the following research question.

How is the structural rigidity, EI, related to the maximum deflection, $|u|$, under different sea and earthquake conditions?

The goal of this paper is to investigate the relation between the rigidity of the windmill and the seismic and water waves. The main effect of interest is the maximum deflection of the windmill. As the electrical components in the top of the windmill can be damaged due to excessive deflection. The maximal allowed deflection is chosen to be $1m$.

In order to model a windmill at sea, the Euler-Bernoulli beam equation is used. The forcing term in this equation is provided by the Morison's equation. This equation models the force of the waves on the windmill. The Morison equation is dependent on the horizontal speed of the waves, which is modelled using the wave equation. Together these equations forms the basic model for a windturbine at sea.

The seismic waves are modelled using a non-homogeneous boundary condition on the bottom of the windmill. At the bottom of the windmill a harmonic oscillation dependent on time alone is prescribed. This is done using the horizontal earthquake model (HEM). This model assumes the seismic wave has fixed amplitude and frequency. The HEM together with the three other component models form the total model.

The relation between the rigidity, EI, and the maximum deflection, $|u|$, is determined using multiple wave and earthquake scenarios. Three wave and earthquake models, each with different severity, are used. This leads to a total of nine scenarios. For each scenario the factor EI, a measure for rigidity, is scaled to ensure the maximal deflection is less than one meter. Based on these scaling factor the relation between the rigidity and maximal deflection is determined.

In Chapter 2 the four component models are explained, these are the Morrison's equation, wave equation, the Euler-Bernoulli equation, and horizontal earthquake model. Additionally, the boundary conditions are detailed in this chapter. In Chapter 3 the model is solved analytically using the method of eigenfunction expansion. Based on this analytical solution the numerical model, called *Windmolentje*, is tested to gain trust in the numerical approximation. In Chapter 4 results of *Windmolentje* are presented and analysed. In Chapter 5 the research question is answered and the validity of the model and results are discussed. The required theorems for mathematical rigor can be found in Appendix B.

2

The model

In this chapter an outline of the general problem is given as well as the used model. A general outline of the problem and model are given in Section 2.1. The model consists of three component models. The relation between these three models is discussed as well. Afterwards in Section 2.2 the Euler-Bernoulli Beam equation is reviewed. In Sections 2.3 and 2.4 the Morison's equation and wave equation are discussed. In Section 2.5 a model for a seismic shock is derived. Subsequently, the boundary conditions are determined in Section 2.6.

2.1. The general problem

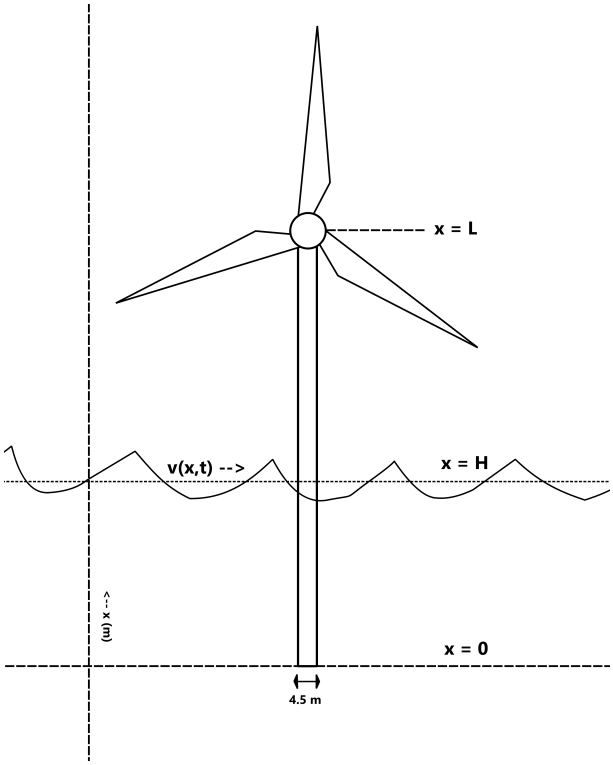

Figure 2.1: Overview of the general situation

The general problem is visualised in Figure 2.1. A windmill, located at sea, is deflected due to the waves. The waves propagate with a velocity of $v(x,t)$ in the horizontal direction. Only a portion of the windmill is placed in the water. With regards to the vertical axis the windmill is placed in water for H

meters. As is common for windmills in the north sea, the windmills are modelled as hollow cylinders with a inner diameter of $4,4m$ and an outer diameter of $4.5m$. The water is modelled as an ideal fluid.

At the bottom of the windmill a seismic wave effects the windmill. This Seismic wave displaces the bottom of the windmill with a fixed frequency and amplitude. This seismic wave is assumed to have no effect on the waves in the water. The seismic wave, windmill, and waves are modelled using four component models.

The model used consists of three component models. The relation between the three components is detailed in Figure 2.2. The Euler-Bernoulli equation models a beam, the beam represents a windmill. This equation is represented by the red box in Figure 2.2. This equation is dependent on a forcing term, the lavender box. This forcing term consists of the force enacted by waves onto the windmill. This forcing term is modelled using the Morison's equation.

The Morison's equation models the drag and inertia force of waves on the windmill. The Morison's equation is dependent on the velocity of the waves. Using linear wave theory a model for the wave velocity is derived, the green box in Figure 2.2. This wave equation completes the model for the windmill.

The seismic wave is modelled using a horizontal earthquake model (HEM). This model assumes the seismic wave to be a harmonic oscillation. Using this model the displacement at the bottom of the windmill is determined. The HEM completes the model.

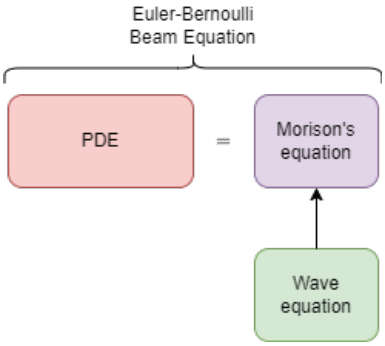

Figure 2.2: Diagram of the relation between the component models.

2.2. Euler-Bernoulli Beam Equation

The first component model is the Euler-Bernoulli beam equation. This equation models the deflection of a beam due to a forcing term. In the sequel a windmill is modelled as a cylindrical beam. As the beam equation is a partial differential equation, the function for the deformation of the beam, with respect to the position in the beam and time, is unknown and is to be solved. The beam equation is as follows:

$$\frac{\partial^2}{\partial x^2}\left(E(x)I(x)\frac{\partial^2 u}{\partial x^2}\right) = -\mu(x)\frac{\partial^2 u}{\partial t^2} + F(x,t). \tag{2.1}$$

If $E(x), I(x)$ and $\mu(x)$ are assumed constant, then equation 2.1 simplifies to the following expression:

$$EI\frac{\partial^4 u}{\partial x^4} = -\mu\frac{\partial^2 u}{\partial t^2} + F(x,t). \tag{2.2}$$

Equation 2.2 consists of a spatial term, temporal term, and forcing term. The spatial term is a fourth order derivative with respect to space which is encapsulated in the variable x. As detailed in Figure 2.1, x takes values ranging from 0 to L. Additionally there are two constants in this term. $E(x)$ is the elastic modulus of the beam material. The windmill is modelled to be constructed by steel. As such, $E = 210\ GPa$ for all x.

The $I(x)$ is the second moment of area. This models the structural strength of the beams shape with respect to the applied force. The second moment of area represents how a set of points are distributed with respect to an axis. The waves forces are working on the windmill on just one side, so only one I is needed on one axis, which will be named I_z. I_z can be calculated with the formula $\int \int_R y^2 dA$, where A is the area of the profile of the windmill. The given windmill has a diameter of $4.5m$ and a thickness of $0.05m$. As the windmill is modelled as a cylindrical beam, the second moment of area is calculated in the following fashion

$$I = \iint_W x^2 dx\, dy = \int_0^{2\pi}\int_{2.2}^{2.25} r^3 \cos^2(\theta) dr\, d\theta = \frac{\pi}{4}(2.25^4 - 2.2^4) \approx 1.73. \tag{2.3}$$

The temporal term consists of a second order derivative with respect to time, t. Multiplied with the constant μ. This term models the mass per unit length of the beam. Using the cylindrical form of the windmill, the value of mu is determined to be $7850 \cdot (2.25^2 - 2.225^2) \cdot \pi$ kg/m. The Forcing term is modelled by the Morison's equation and is detailed below.

To solve this equation for a specific windmill, the external forces $F(x,t)$ on the windmill are needed. The forces working on this windmill are waves, whose forces are given by the Morrison Equation. This equation will be further specified in section 2.3. In the sequel $E(x), I(x)$ and $\mu(x)$ are assumed constant.

2.3. Morison Equation

The Morison equation describes the behaviour of an oscillatory flow interacting with a body (like a windmill). The equation is as follows:

$$F(x,t) = \pi R^2 \rho\,(1 + C_a) v_t + \rho\, C_d R\, v\, |v|. \tag{2.4}$$

This equation consists of two forces. $\pi R^2 \rho\,(1 + C_a) v_t$ is the inertia force. This force is caused by the amount of water displaced by the beam.

Then $\rho\, C_d R\, v\, |v|$ is the drag force. The windmill moving relatively opposite to the wave movement generates this drag force. This force depends on the wave velocity squared. However, the direction of the waves is of importance. As such, the term $v \cdot |v|$ is used. For a full derivation of this model the reader is advised to review [2].

In the Morison's equation, several parameters are present. $F(x,t)$ denotes the force of the Morison's equation. This force is dependent on the wave velocity denoted by v. v_t is the derivative of the flow velocity with respect to time, thus the flow acceleration.

The density ρ is the sea water density. This constant is determined to be $1030 kg/m^3$. For steel, the density, denoted by ρ_{steel}, is chosen to be $7850 kg/m^3$.

A is the cross section area of the windmill per unit length. This geometric parameter is determined to be

$$\pi {R_2}^2 - \pi {R_1}^2 = \pi \cdot 2.25^2 - \pi \cdot 2.2^2 \approx 0.6990. \tag{2.5}$$

C_a denotes the added mass coefficient. Added mass is additional mass generated by the windmill deflecting the waves moving around it. As the windmill and the water cannot occupy the same space at the same time, this coefficient is used to scale the mass of the water to model the windmill mass. As such, the added mass coefficient is the ratio between the mass per unit length of the windmill and the displaced mass per unit length of the water. This term is determined to be

$$C_a = \frac{\rho_{steel}\, \pi \cdot \left({R_2}^2 - {R_1}^2\right)}{\rho_{sea}\, \pi \cdot R_2^2} = \frac{\rho_{steel}\, A}{\rho_{sea}\, \pi\, 2.25^2} \approx 0.33496. \tag{2.6}$$

2.4. Wave Equation

The motion of water particles of waves in the sea are described by the wave equation. Two types of waves are possible, short waves, affected by the wind and gravity, and long waves, which can be found at seashores. The windmill is assumed to be distant from seashores, as such the long waves are disregarded. The equation is restricted to only short waves.

The vertical velocity is disregarded, as the vertical movement generates no force onto the windmill. As such the horizontal component further analysed. The wave equation is derived from a PDE. The PDE and its solution are detailed in [5].

As detailed in [5], the wave velocity is shown to have a potential. Thus $v = \nabla\phi$, where ϕ is the potential of v. The horizontal component of the wave velocity is determined to be

$$v(x,t) \equiv \left.\frac{\partial \phi}{\partial \chi}\right|_{\chi=0} = \sigma a \frac{\cosh(kx)}{\sinh(kH)} \cos(\sigma t). \tag{2.7}$$

Here χ is vertically orientated. Multiple parameters are present. These are determined to have different values.

The frequency of the waves is set to $\frac{2\pi}{T}$. Here T is the corresponding wave period, T is set to either $5.7, 8.6$ or 11.4 corresponding to the scenario of ocean (mild, medium or rough respectively). a is the amplitude of the waves. These terms dictate the oscillatory behaviour of the wave velocity.

k is chosen as $\frac{2\pi}{\lambda}$. This is the wave number. λ is the wave length and set to either $33.8m, 76.5$ or 136 [1]. In the denumerator a sinh is present. This term is dependent on the depth of the sea. This length is set to $50m$ and denoted by H. For further detail, the reader is advised to review the lecture nothes of H.E Swart[5].

2.5. Horizontal earthquake model

Alongside the model for the windmill, a model for a seismic shock is constructed. This is modelled using a horizontal earthquake model (HEM). The seismic wave is assumed to be oscillatory. As such, the earthquake is modelled as a harmonic oscillation at the ocean floor, this translates into a boundary condition at the $x = 0$.

Boundary conditions are further discussed below, including that of the model with earthquake.

2.6. Boundary conditions

In order to solve the Euler-Bernoulli beam equation, the boundary conditions are to be determined. As the PDE is of fourth order, four boundary conditions are to be determined. As the PDE has an interval as domain, for two points boundary conditions are to be specified.

Boundary conditions at the bottom

In the basic model the windmill is fixed at the bottom and stationary. The bottom of the windmill is not capable of changing angle, as such the first two boundary conditions are

$$u(0,t) = 0, \quad \frac{\partial u}{\partial x}(0,t) = 0. \tag{2.8}$$

Boundary conditions at the top

The top of the model is allowed to move freely. As no external force is acting on the top of the windmill, the spatial derivatives at L take on the following form,

$$\frac{\partial^2 u}{\partial x^2}(L,t) = 0, \quad \frac{\partial^3 u}{\partial x^3}(L,t) = 0 \tag{2.9}$$

Initial conditions

Initially the windmill is modelled as being stationary. As such, initially there is no deformation or change in deformation. This is captured by the following initial conditions.

$$u(x,0) = 0, \quad \frac{\partial u}{\partial t}(x,0) = 0. \tag{2.10}$$

Seismic wave boundary condition

The model for the deflection due to a seismic wave derived in Section 2.5, is implemented as a boundary condition to model the deflection caused by a seismic wave. As the seismic wave displaces the wind-turbine at its bottom, this non-homogeneous boundary condition is modelled as

$$u(0,t) = A_0 \cdot cos(\omega t). \tag{2.11}$$

Where A_0 is the amplitude of the earthquake, and ω the frequency. The angle of displacement of the windmill at its bottom is still modelled to be constant. This leads to the following boundary condition

$$u_x(0,t) = 0. \tag{2.12}$$

The final model

The formulation of the boundary conditions due to the seismic shock, leads to the formulation of the final model. This final model is of the form

$$EI\frac{\partial^4 u}{\partial x^4} = -\mu\frac{\partial^2 u}{\partial t^2} + F(x,t), \quad \begin{cases} \text{BC: } u(0,t) & = A_0 \cdot cos(\omega t), \quad \dfrac{\partial u}{\partial x}(0,t) = 0 \\ \text{BC: } \dfrac{\partial^2 u}{\partial x^2}(L,t) & = 0, \quad \dfrac{\partial^3 u}{\partial x^3}(L,t) = 0 \\ \text{IC: } u(x,0) & = 0, \quad \dfrac{\partial u}{\partial t}(x,0) = 0. \end{cases} \tag{2.13}$$

2.7. Summary

To summarise, there are four equations required to formulate the basic model. The Euler-Bernoulli beam equation details how a beam is deflected by external forces acting on the beam. This beam represents a windmill in the basic model. The Euler-Bernoulli beam equation contains a term detailing the force acting on the beam. This term is detailed by the Morison equation. This equation models how an oscillatory flow interacts with a cylinder. In turn, the Morison equation requires a term for the flow velocity. This flow velocity is modelled using the wave equation.

The effect of a seismic shock on the windmill is modelled using the horizontal earthquake model. This model assumes the seismic shock to be a harmonic oscillation. Using these models both homogeneous and non-homogeneous boundary and initial conditions are determined. The homogeneous system models the windmill without the seismic wave, and the non-homogeneous model the windmill with the effect of a seismic shock.

3

Analytical model

In this chapter, an analytical solution to Problem 2.13 is constructed. This problem can be solved using the method of seperation of variables. The problem is first solved for an arbitrary forcing $F(x,t)$ with earthquakes. Then, for $F = 0$ and a single earthquake acting, a full analytical solution is constructed to gain insight into the problem and the influence of the various beam parameters. This full analytical solution is then used to verify and gain confidence in the numerical model called *Windmolentje*.

3.1. Dependency graph of the problem

In the below figure the solution of the problem is outlined as a dependency graph. The various colors indicate dependency on space, time or none. To construct the solution $u(x,t)$, one needs the eigenfunctions $\phi_n(x)$ and the time coefficients $b_n(t)$. It will turn out that the time coefficients depend solely on a so-called *Resonance Integral*, denoted as Rs. The resonance integral together with the eigenfunction coefficients $\widehat{F}_n$ will turn out to be the main bottleneck in finding analytical solutions.

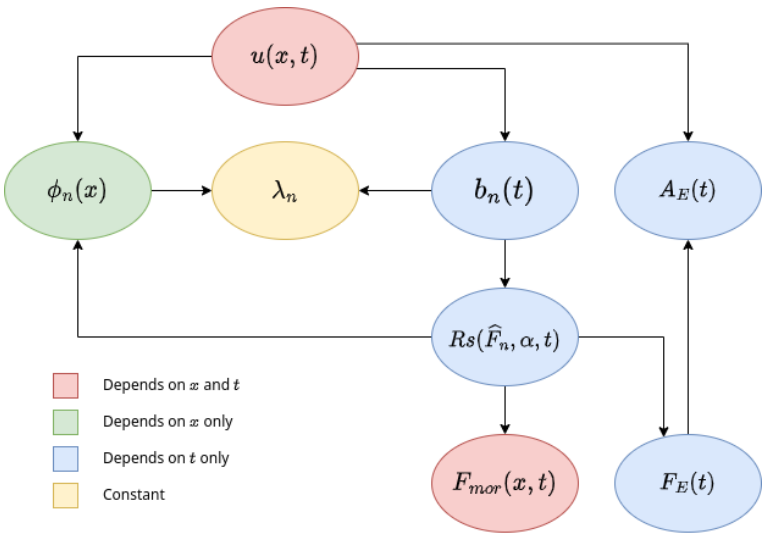

Figure 3.1: Dependency tree

3.2. Reducing to homogeneous boundaries

Since the problem for $u(x,t)$ has inhomogeneous boundary conditions, the problem has to be reduced to a homogeneous boundary conditions for $v(x,t)$. To this end, let $v(x,t)$ be given by

$$v(x,t) = u(x,t) - A_E(t), \tag{3.1}$$

then $v(x,t)$ now satisfies homogeneous boundary conditions due to the subtraction of $A_E(t)$. The differential equation for $v(x,t)$ then becomes

$$\frac{\partial^2 v}{\partial t^2} + {A_E}'' = -\frac{EI}{\mu}\frac{\partial^4}{\partial x^4}(v + A_E) + \frac{F}{\mu} \tag{3.2}$$

$$\frac{\partial^2 v}{\partial t^2} = -\frac{EI}{\mu}\frac{\partial^4 v}{\partial x^4} + \frac{F - \mu {A_E}''}{\mu} \tag{3.3}$$

Let the new forcing term be redefined as $F_{tot}(x,t) = F(x,t) - \mu {A_E}''(t)$, then the full problem for $v(x,t)$ is

$$\frac{\partial^2 v}{\partial t^2} = -\frac{EI}{\mu}\frac{\partial^4 v}{\partial x^4} + \frac{F_{tot}}{\mu}, \tag{3.4}$$

subject to the full homogeneous boundary conditions and initial conditions

$$\begin{aligned} v(0,t) &= 0, & \frac{\partial v}{\partial x}(0,t) &= 0 \\ \frac{\partial^2 v}{\partial x^2}(L,t) &= 0, & \frac{\partial^3 v}{\partial x^3}(L,t) &= 0 \\ v(x,0) &= 0, & \frac{\partial v}{\partial t}(x,0) &= 0. \end{aligned} \tag{3.5}$$

Once the problem for $v(x,t)$ is solved, the final solution for $u(x,t)$ can be found as $u(x,t) = v(x,t) + A_E(t)$.

3.3. Determining the eigenfunctions

To solve for the non-homogeneous forcing problem, the solution $v(x,t)$ has to be expanded in an infinite sum of eigenfunctions ϕ_n corresponding to the homogeneous forcing problem. These eigenfunctions are determined from

$$\frac{\partial^2 v}{\partial t^2} = -\frac{EI}{\mu}\frac{\partial^4 v}{\partial x^4}. \tag{3.6}$$

Applying seperation of variables and letting $\nu(x,t) = \phi(x)G(t)$ yields

$$\begin{aligned} \phi\frac{\partial^2 G}{\partial t^2} &= -\frac{EI}{\mu}\frac{\partial^4 \phi}{\partial x^4}G \\ -\frac{\partial^2 G}{\partial t^2}\frac{\mu}{EIG} &= \frac{\partial^4 \phi}{\partial x^4}\frac{1}{\phi} = \lambda^4 \end{aligned} \tag{3.7}$$

The separation constant λ^4 has been proven to be real and positive in Theorem B.3.1. A fourth power is used to clarify the sign and simplify future computations with powers. From this equation, the differential equation for ϕ can be formulated as

$$\frac{d^4\phi}{dx^4} = \phi\lambda^4, \quad \text{subject to} \quad \begin{cases} \phi(0) = 0 & \phi'(0) = 0, \\ \phi''(L) = 0 & \phi'''(L) = 0. \end{cases} \tag{3.8}$$

This differential equation can be solved by substituting $\phi(x) = e^{rx}$, yielding the following four roots,

$$\begin{gathered} r^4 = \lambda^4 \\ r^2 = \lambda^2 \quad \vee \quad r^2 = -\lambda^2 \\ r = \lambda \quad \vee \quad r = -\lambda \quad \vee \quad r = i\lambda \quad \vee \quad r = -i\lambda. \end{gathered} \tag{3.9}$$

These roots yield two exponential terms and two periodic terms for ϕ. Combining all four solutions gives the general solution.

$$\phi(x) = Ae^{\lambda x} + Be^{-\lambda x} + C\cos(\lambda x) + D\sin(\lambda x). \tag{3.10}$$

To simplify computations and expressions, the exponential terms can be replaced by $\cosh(\lambda x)$ and $\sinh(\lambda x)$. This yields a simplified general solution.

$$\phi(x) = A\cosh(\lambda x) + B\sinh(\lambda x) + C\cos(\lambda x) + D\sin(\lambda x). \tag{3.11}$$

The next step is to apply the boundary conditions to find the constants. The first boundary conditions to apply are those for $x = 0$.

$$\left.\begin{matrix} \phi(0) = 0 \\ \phi'(0) = 0 \end{matrix}\right\} \quad \Rightarrow \quad \begin{matrix} A = -C \\ B = -D \end{matrix} \tag{3.12}$$

Substituting this back reduces ϕ to two arbitrary constants.

$$\phi(x) = A(\cosh(\lambda x) - \cos(\lambda x)) + B(\sinh(\lambda x) - \sin(\lambda x)). \tag{3.13}$$

The final two boundary conditions yield a system of two equations for ϕ. This system eliminates another constant for ϕ.

$$\left.\begin{matrix} \phi''(L) = 0 \\ \phi'''(L) = 0 \end{matrix}\right\} \quad \Rightarrow \quad \begin{cases} A\left(\cosh(\lambda L) + \cos(\lambda L)\right) + B\left(\sinh(\lambda L) + \sin(\lambda L)\right) & = 0, \\ A\left(\sinh(\lambda L) - \sin(\lambda L)\right) + B\left(\cosh(\lambda L) + \cos(\lambda L)\right) & = 0. \end{cases} \tag{3.14}$$

Expressing B in terms of A yields the following expression for λ.

$$B = -A\frac{\cosh(\lambda L) + \cos(\lambda L)}{\sinh(\lambda L) + \sin(\lambda L)} \tag{3.15}$$

$$\left(\sinh(\lambda L) - \sin(\lambda L)\right)\left(\sinh(\lambda L) + \sin(\lambda L)\right) - \left(\cosh(\lambda L) + \cos(\lambda L)\right)^2 = 0. \tag{3.16}$$

Simplifying this expression yields the final transcendental equation for λ_n. Where due to the periodicity of cos, there exist infinitely many λ_n,

$$\cosh(\lambda_n L)\cos(\lambda_n L) + 1 = 0. \tag{3.17}$$

The solutions to this transcendental equation can be found by substituting

$$\begin{aligned} \gamma_n &= \lambda_n L \\ \cosh(\gamma_n)\cos(\gamma_n) + 1 &= 0, \end{aligned} \tag{3.18}$$

and then proceeding to solve numerically for γ_n. The value of λ_n can then be found from the above equality. The γ_n are constant and not dependent on any variables. They can be considered as the base eigenvalues of beams of any length, since the real eigenvalues are just scaled versions of γ_n.

The final solution for $\phi_n(x)$ can be summarized as follows.

$$\begin{cases} \phi_n(x) &= \cosh(\lambda_n x) - \cos(\lambda_n x) - C_n\left(\sinh(\lambda_n x) - \sin(\lambda_n x)\right), \\ C_n &= \dfrac{\cosh(\gamma_n) + \cos(\gamma_n)}{\sinh(\gamma_n) + \sin(\gamma_n)}. \end{cases} \tag{3.19}$$

This is the space solution for the homogeneous problem.

3.3.1. Numerical influence on the eigenfunctions

The eigenfunctions determined in the previous section cause problems numerically. This happens because numerically subtracting two high order terms causes rounding errors. In ϕ_n, these terms are $\sinh(\lambda_n x)$ and $\cosh(\lambda_n x)$. The following plot visualizes the issue.

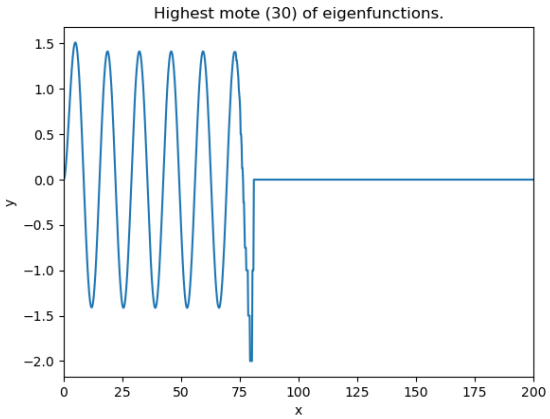

Figure 3.2: Floating point error in mode 30.

The solution to this problem is to collect all high-order terms of $e^{\lambda_n x}$ together analytically. Removing the hyperbolic sine and cosines from ϕ_n results in the numerically favorable expression

$$\phi_n(x) = \frac{(1 - C_n)e^{\lambda_n x} + (1 + C_n)e^{-\lambda_n x}}{2} + C_n \sin \lambda_n x - \cos \lambda_n x. \tag{3.20}$$

As $\lambda_n x \to \infty$ only a single high-order term $e^{\lambda_n x}$ remains. Observing the same plot motivates writing ϕ_n in this new form.

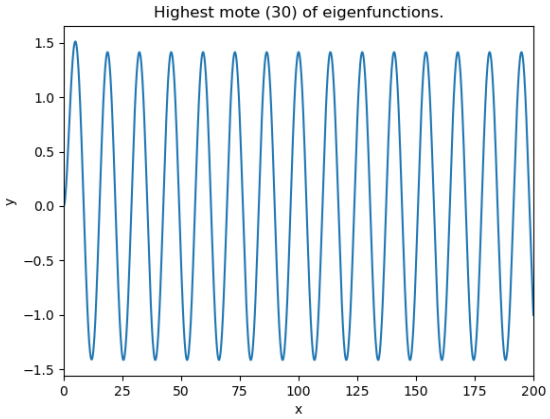

Figure 3.3: Mode 30 with simplified eigenfunction expression.

3.4. Determining the time coefficients

With the eigenfunctions determined, the problem with non-homogeneous forcing for v can be solved. To this end, v is expanded as an infinite sum over the eigenfunctions $\phi_n(x)$ with time-dependent coefficients called $b_n(t)$.

$$v(x,t) = \sum_n b_n(t)\phi_n(x). \tag{3.21}$$

Since both v and ϕ_n satisy the same homogeneous boundary conditions, differentiation and summation can be interchanged. This justifies inserting $v(x,t)$ in Equation 3.4, which results in the differential equation for b_n.

$$\begin{aligned} \sum_{n=1}^{\infty} {b_n}''\phi_n &= -\frac{EI}{\mu}\sum_{n=1}^{\infty} b_n \frac{d^4\phi}{dx^4} + \frac{F_{tot}}{\mu} \\ \sum_{n=1}^{\infty}\left({b_n}'' + \frac{EI}{\mu}{\lambda_n}^4 b_n\right)\phi_n &= \frac{F_{tot}}{\mu} \end{aligned} \tag{3.22}$$

Thus b_n can be found as the eigenfunction coefficient of F_{tot}. This results in the differential equation

$$\begin{aligned} {b_n}'' + \frac{EI}{\mu}{\lambda_n}^4 b_n &= \frac{\widehat{F}_{tot,n}}{\mu}, \\ b_n(0) &= 0, \\ {b_n}'(0) &= 0. \end{aligned} \tag{3.23}$$

The notation $\widehat{f_n}$ is used to denote the n-th coefficient of f expanded around the eigenfunctions ϕ_n.

$$\widehat{f_n} = \frac{\int_0^L f\phi_n dx}{\int_0^L {\phi_n}^2 dx} = \frac{1}{L}\int_0^L f\phi_n dx, \tag{3.24}$$

The integral of ${\phi_n}^2$ over its domain can be shown using a computer algebra system to be constant and equal to L.

The differential equation for b_n can be solved using the method of variation of parameters. Observe that b_n is in standard-form and hence the homogeneous problem for y_n becomes

$$y_n{}'' + \frac{EI}{\mu}{\lambda_n}^4 y_n = 0. \tag{3.25}$$

Since the constants μ, E, I and ${\lambda_n}^4$ are positive, the solution for the homogeneous problem is periodic and given by

$$y_n(t) = A_n \cos(\alpha_n t) + B_n \sin(\alpha_n t). \tag{3.26}$$

Here the eigenfrequencies of the beam become apparent and are defined as α_n.

$$\alpha_n = \sqrt{\frac{EI{\lambda_n}^4}{\mu}}. \tag{3.27}$$

Since all initial conditions are set to zero, the constants A_n and B_n become zero and b_n equals the particular solution from variation of parameters.

$$b_n(t) = -\frac{1}{\mu\alpha_n}\cos(\alpha_n t)\int_0^t \widehat{F}_{tot,n}(\bar{t})\sin(\alpha_n \bar{t})d\bar{t} + \frac{1}{\mu\alpha_n}\sin(\alpha_n t)\int_0^t \widehat{F}_{tot,n}(\bar{t})\cos(\alpha_n \bar{t})d\bar{t} \tag{3.28}$$

Combining all terms under a single integral and using the trigonometric identity

$$\sin(x-y) = \sin(x)\cos(y) - \cos(x)\sin(y), \tag{3.29}$$

yields for $b_n(t)$ the compact expression

$$b_n(t) = \frac{1}{\mu\alpha_n}\int_0^t \widehat{F}_{tot,n}(t-\bar{t})\sin(\alpha_n \bar{t})d\bar{t}. \tag{3.30}$$

This is a convolution integral with the eigenfunction coefficients of the force F_{tot} and a sine wave. Since this integral is so pivotal in the time evolution of the windturbine aswell as the presence of resonance, it will be defined as the *Resonance Integral* $Rs(f,\alpha,t)$ given by

$$Rs(f,\alpha,t) = \int_0^t f(t-\bar{t})\sin(\alpha\bar{t})d\bar{t} \tag{3.31}$$

Introducing the resonance integral to b_n yields the final solution in very compact form given by

$$b_n(t) = \frac{Rs(\widehat{F}_{tot,n},\alpha_n,t)}{\mu\alpha_n} \tag{3.32}$$

3.5. Final solution

Now that all components of the solution $u(x,t)$ are determined, the final solution for the deflection of a windturbine subject to the combined forcing $F_{tot}(x,t) = F(x,t) - \mu {A_E}''(t)$ of an arbitrary force F and an earthquake force is given by

$$u(x,t) = A_E(t) + \sum_{n=1}^{\infty}\frac{Rs(\widehat{F}_{tot,n},\alpha_n,t)}{\mu\alpha_n}\phi_n(x) \tag{3.33}$$

Since the earthquake force is only dependent on time, its eigenfunction coefficient can be simplified. The earthquake force for m earthquakes with frequency ω_n and amplitude A_n is given by

$$-\mu {A_E}''(t) = \mu \sum_{i=1}^{m} A_i {\omega_i}^2 \cos(\omega_i t) \tag{3.34}$$

Then the eigenfunction coefficients of the total earthquake force is given simply by

$$\begin{aligned} -\mu \widehat{A_{E,n}}'' &= -\frac{\mu}{L} \int_0^L {A_E}''(t) \phi_n(x) dx \\ &= -\mu {A_E}'' \frac{1}{L} \int_0^L \phi_n dx \\ &= \mu \beta_n \sum_{i=1}^{m} A_i {\omega_i}^2 \cos(\omega_i t) \end{aligned} \tag{3.35}$$

The β_n are constants and can be shown to be dependent only on γ_n, which in turn is not dependent on any physical parameters of the windturbine.

$$\beta_n = \frac{1}{L} \int_0^L \phi_n dx \tag{3.36}$$

The resonance integral for the earthquake eigenfunction coefficients requires the resonance integral of a single cosine. This can be solved for analytically and is found to be

$$Rs(\cos(\omega t), \alpha, t) = \alpha \frac{\cos(\omega t) - \cos(\alpha t)}{\alpha^2 - \omega^2} \tag{3.37}$$

Substituting the earthquake eigenfunction coefficients back into the expression for $u(x,t)$ given by Equation 3.33 and using the linearity of the resonance integral yields the analytical solution for $u(x,t)$ as far as analytical solving goes.

$$u(x,t) = A_E(t) + \sum_{n=1}^{\infty} \frac{1}{\mu \alpha_n} \left(Rs(\widehat{F}_n, \alpha_n, t) + \mu \beta_n \sum_{i=1}^{m} A_i {\omega_i}^2 \alpha_n \frac{\cos(\omega_i t) - \cos(\alpha_n t)}{{\alpha_n}^2 - {\omega_i}^2} \right) \phi_n(x) \tag{3.38}$$

Where in the case for this project the external force F is given by the Morison force F_{mor}.

3.6. Verification of the numerical model

To gain confidence in the numerical model *Windmolentje* and to verify its workings, a single case of the analytical model from Equation 3.38 is considered. The external forces F are set to zero, and a single earthquake of amplitude $A = 1$ and frequency $\omega = 2\pi$ (1 Hz) is enabled. For a single earthquake, the analytical solution gives

$$u(x,t) = A \cos(\omega t) + \sum_{n=1}^{\infty} \beta_n A \omega^2 \frac{\cos(\omega t) - \cos(\alpha_n t)}{{\alpha_n}^2 - \omega^2} \phi_n(x). \tag{3.39}$$

Below, the solution from *Windmolentje* and the analytical solution in Maxima are plotted next to each other.

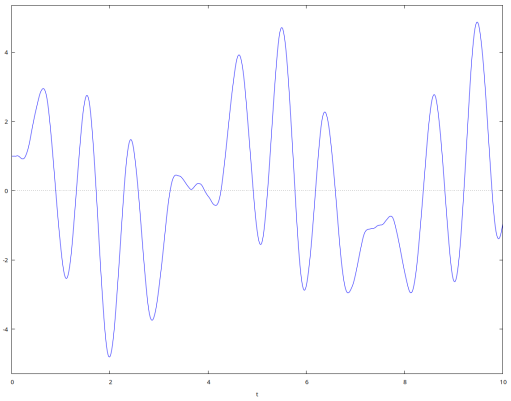

(a) Analytical solution

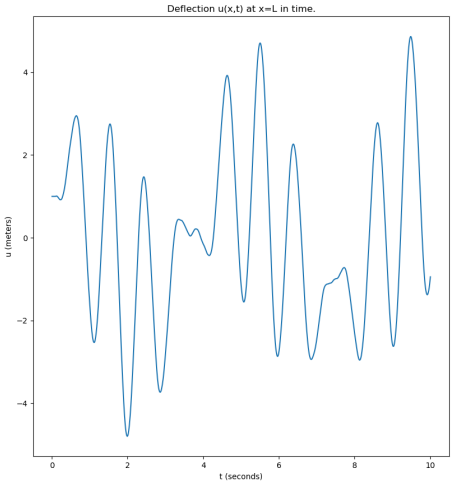

(b) *Windmolentje* solution

From the matching shape and amplitudes of these graphs, there is a degree of a confidence in the numerical model *Windmolentje*. This is the green light to apply *Windmolentje* to cases where analytical methods are no longer feasible, which brings us to the next section.

4

Results

In this chapter the results of the model with earthquake are detailed and analysed. In Section 4.2 an overview of the results is given and the different scaling factors are analysed. Subsequently, in Section 4.2.1 the different results are compared. A summary is provided in Section 4.4.

4.1. Table of eigenfrequencies

The below table gives the eigenfrequencies of a windturbine subject to the default material properties and parameters, these can be used to explain the excitation of various modes. Note however that these frequencies will change for different material settings, which is the case for various results in this section. Still, this table can get an idea of the order of the eigenfrequencies.

Mode	Eigenfrequency (Hz)
1	0.20
2	1.26
3	3.55
4	6.95
5	11.50
6	17.18
7	24.00
8	31.95
9	41.05
10	51.27

Table 4.1: Eigenfrequencies of modes for a standard windturbine

4.2. Scaling factors

Having formulated an analytical solution the Euler-Bernoulli beam equation with non-homogeneous BC, the solution can be numerically computed and analysed. To answer the research question, the maximum deflection was examined in a time period of 60 seconds, across 9 different scenarios. There were three scenarios of waves, and three scenarios of earthquakes, leading to 9 combinations. The three scenarios of the waves had three parameters, wave period, wave length and amplitude. Which are described in Table 4.2.

Scenario	Period	Amplitude	Wavelength
Mild	5.7	1.5	33.8
Medium	8.6	4.1	76.5
Rough	11.4	8.5	136

Table 4.2: The period, amplitudes and wavelength associated with the different wave types.

The three scenarios of earthquakes were; no earthquake, mild earthquake, and a heavy earthquake. Both earthquakes consisted of multiple frequencies. This to try and make the shake a bit more chaotic as in real life. The different earthquakes correspond to different BC in the following fashion.

- Earthquake scenario I corresponds to a homogeneous boundary condition.
- Earthquake scenario II is a boundary condition of: $\cos(2\pi \cdot 0.1t) + 0.5\cos(2\pi t) + 0.1\cos(2\pi \cdot 10t)$.
- Earthquake scenario III is a boundary condition of: $2\cos(2\pi \cdot 0.1t) + 1\cos(2\pi t) + 0.2\cos(2\pi \cdot 10t)$.

A mild ocean and no earthquake is assumed to be the base case. Using Windmolentje, this scenario resulted in a maximum deflection of $0.66m$. The assumed maximum allowed deflection is $1m$.

After this all other scenarios were also run, and where needed EI was adjusted until the maximum deflection was within the allowed safety bounds of $\leq 1m$. Here it is useful to note deflection is being measured as compared to the position of the bottom of the wind turbine, as this is moving along with the ocean floor. In a perfectly rigid beam, it would oscillate horizontally but the entire beam would still be perfectly straight.

Now a table is shown where all scenarios can be seen with their adjusted (if needed) EI. Note here that the base case was within safety bounds, all other EI the factors by which they needed to be adjusted.

	No earthquake	Mild earthquake	Heavy earthquake
Mild Waves	1	100	200
Medium Waves	1	100	500
Rough Waves	1	75	1000

Table 4.3: Scaling factors corresponding to different scenarios.

As can be seen in Table 4.3 the earthquake warrants a scaling factor in the order of 10^2 with mild waves. This scaling factor increases, but the order of the scaling remains the same for medium waves. For rough waves the scaling factor increases to 10^3.

For mild and medium waves the scaling factor increases significantly with an increase in earthquake severity. For no and mild earthquakes an increase in wave severity has little effect on the scaling factor. Notably, for rough waves and mild earthquakes the scaling factor decreases when compared to medium waves and a mild earthquake.

4.2.1. Effect earthquake and wave cancellation on EI scaling

The scaling factor for rough waves and mild earthquakes does not follow the pattern of the rest of the data. As such, this phenomenon is to be scrutinised further. To this end the mode excitation of the first ten modes is analysed together with the size of the Morison and earthquake force. Figure 4.1 visualised both factors over time.

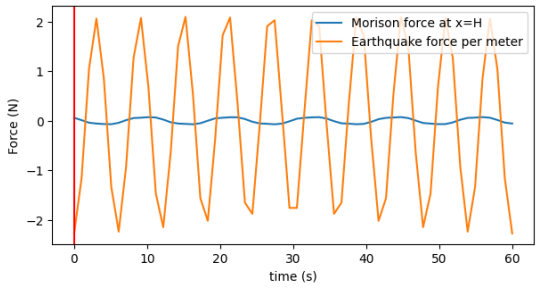

(a) Size of Morison force and earthquake force in $10^6 N$ over time.

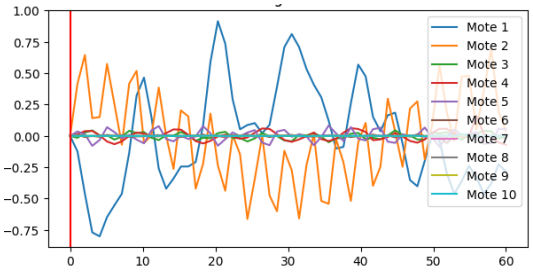

(b) Excitation of different modes over time.

Figure 4.1: Figure detailing mode excitation and force size over time.

As can be seen in Figure 4.1b the earthquake force in combination with the Morison force excites mode 1 and mode 2 noticeably. Note that the excitation of the two modes occur opposite to each

other. Initially mode 2 has a positive excitation and mode 1 a negative excitation. Subsequently, as the excitation of mode 2 decreases and becomes negative, the excitation of mode 1 increases and becomes positive. The oscillatory behaviour of the two curves are opposite. The excitement of mode 1 can also be explained from Table 4.1. The frequency of an earthquake of 0.1 Hz comes very close to the eigenfrequency of mode 1 for the standard windturbine of 0.22 Hz.

4.3. Numerical error

As can be seen in Figures 4.1a 4.1b the graphs are not smooth. This is due to a lack of numerical precision. The numerical precision for the integrals is set to be $1.49 \cdot 10^{-8}$ in absolute error using a quadrature method from *scipy*. For sampling the graphs, 60 samples we're taken over an interval of 60 seconds. This means one sample equals a single second. This number of samples still captures the most vital information of the simulation while retaining decent speed.

4.4. Summary

Using nine different scenarios, the relation between the rigidity and seismic and water waves was detailed. The results are tabulated in Table 4.3. Overall an increase in severity of earthquakes or wave force warranted a larger scaling factor to accommodate for this.

For a mild earthquake and rough waves, two different modes were excited in an opposite fashion. This excitation does not coincide with the curve of the forces individually.

5

Conclusion and discussion

Having answered the research question, conclusions can be formulated based on the found results. In this Chapter these conclusions will be given. Additionally, the validity of the results and research process will be discussed. The research question was as follows.

How is the structural rigidity (EI) related to the maximum deflection, $|u|$, under different sea and earthquake conditions?

5.1. Conclusion

As detailed in table 4.3, an increase in earthquake severity leads to a greater increase in scaling factor compared to an increase in wave severity. Solely the waves, without earthquakes, do not deflect the beam sufficiently to damage it. This much can be concluded as the scaling factor being 1.

Combinations of earthquakes and stronger waves result in a higher needed structural rigidity, but this is not always the case. As can be seen in Table 4.3 for a mild earthquake and rough waves. Due to the excitation of two opposite modes, detailed in Figure 4.1b, the deflection of the beam is mitigated. This is due to the chosen frequencies in the model. As such, if these frequencies do align, stronger forces will occur on the windmill, therefore resulting in a higher maximum deflection. Else, the waves forces will barely have any influence on the earthquake forces.

So to answer the research question, the needed structural rigidity really depends on the situation. Stronger waves don't necessarily lead to a higher EI, only if an earthquake is also active. Stronger earthquakes, however, do lead to a higher EI.

5.2. Discussion

During this paper multiple assumptions were made. In order to strengthen the validity of this paper, these assumption and their consequences are discussed. In addition, numerous further research suggestions are made.

As detailed in Chapter 2 the windmill is assumed to be a hollow cylinder. As such, the shape of the model windmill does not coincide with the actual shape of windmills. As the shape of actual windmills is more conic, the elastic modulus, second moment of area, and mass per unit length become functions of space. This can lead to different behaviour of the windmill due to water and seismic waves. As this discrepancy between the model and an actual windmill was noted, it does not effect the validity of the results in this report. The validity of the used model does decrease due to this discrepancy. Further research is suggested into the model with non-constant coefficients in the Euler-Bernoulli beam equation.

The HEM detailed in Section 2.5 does not into account the relation between a seismic wave and ocean waves. As such, the results do not necessarily mirror the effect seismic waves have on windmills. As seismic waves can alter the amplitude and frequency of waves, the relation between the seismic wave

and ocean waves is to be taken into account for a realistic model. Additionally, as the HEM assumes the seismic wave to be a harmonic oscillation with a fixed frequency and amplitude, the model need not coincide with actual earthquakes. Both factors do no effect validity of the results, as these factors have been stated. However, this does effect the validity of the used model. As such, further research taking these two factors into account is suggested.

As for the numerical model *Windmolentje*, it went through a few cycles of improvement until it is at its current state. One of the first hurdles was the eliminating of numerical imprecision in hyperbolic functions. This caused issues with computing eigenfunctions of modes greater than 10. Our solution of combining higher order terms resolved this issue. Also a single missed divison by a constant in the numerical model can yield deflections of unrealistic proportions, which cost much time to find and resolve. Another numerical challenge presented it self during integration. If the frequencies inside the resonance integral become large enough (greater than 1000), then computing the resonance integral numerically requires additional effort. A numerical integrator is not adapted to work with high-frequency harmonic functions. To solve such issues, a special integrator should be used, or the integral should be split in pieces to maintain sufficient precision. In this project, these higher frequency integrals we're of no concern since all eigenfrequencies fell roughly below 200 if taking 10 modes or less.

One further optimisation that we did not utilize in our numerical computations is the fact that the Morison force is seperable in space and time. This would allow the computation of the eigenfunction coefficient to be optimised by precomputing the integrals of the spatial component and eigenfunctions, in the same manner as we did for the β_n constants used for the earthquakes. This eliminates one integral when evaluating the deflection at a certain time t, leaving only the resonance integral of an absolute cosine.

An improvement to the waves in this report is to consider stacked Morison forces of different frequencies and amplitude for a more realistic setting. The current model assumes the waves to be of a single period, amplitude and wavelength, which can impair the occurence of resonance. A rough ocean in a realistic setting consists of multiple layers of waves with high frequency ripples and low frequency tall waves. This mix of frequencies can change the excitation of eigenfunctions of the windturbine and thus might yield better predictions on the stability.

References

[1] BCcampus. *Waves*. URL: https://opentextbc.ca/geology/chapter/17-1-waves/.

[2] J. Journée and W. Massie. *OFFSHORE HYDROMECHANICS*. 1st ed. Delft University of Technology, 2001.

[3] Arim Kaynia. “Seismic considerations in design of offshore wind turbines”. In: *Science direct* 124 (2019), pp. 399–407.

[4] Statista. *Distribution of electricity generation worldwide in 2022, by energy source*. 2023. URL: https://www.statista.com/statistics/269811/world-electricity-production-by-energy-source/#:~:text=In%5C%202022%5C%2C%5C%20coal%5C%20accounted%5C%20for,for%5C%20electricity%5C%20generation%5C%20in%5C%202021. (visited on 04/27/2023).

[5] H.E de Swart. *Ocean Waves*. 1st ed. University of Utrecht, 2015.

A

Source Code

In this appendix the code used in this report are linked. The reader is advised to view the GitHub for the code https://github.com/parcevval/pde-beam-equation. If the reader wishes to contact the writers regarding the code, this can be done mailto:fvandertop@gmail.com.

B

Theorems

When deriving and solving the basic model several theorems regarding the partial differential equation (PDE) were used. In this chapter these theorems are proven and further detailed.

B.1. Self-adjoint operator

The Euler-Bernoulli beam equation contains two linear operators. The spacial operator is of special interest for this problem. For the Euler-Bernoulli beam equation, when assuming the elastic modulus and second moment of area to be constant, the spacial operator is as follows.

$$L := \frac{\partial^4}{\partial x^4} \tag{B.1}$$

The self-adjoint property of this operator is to be proven.

Theorem B.1.1. *The spacial operator L is self-adjoint.*

Proof. In order to prove the self-adjoint property for L an intermediate result is required. This being the Lagrange identity. This identity is of the following form. For u, v the following holds true.

$$\frac{d}{dx}\bigg(- \frac{\partial u}{\partial x}\frac{\partial^2 v}{\partial x^2} + u\frac{\partial^3 v}{\partial x^3} - v\frac{\partial^3 u}{\partial x^3} + \frac{\partial v}{\partial x}\frac{\partial^2 u}{\partial x^2}\bigg) = u\frac{\partial^x 4}{\partial v^x} - v\frac{\partial^x 4}{\partial u^x} \tag{B.2}$$

This identity is shown to be correct by direct computation.

Suppose u and v are two functions which both satisfy the same boundary conditions on $[a, b]$. Then the following holds true.

$$\bigg[- \frac{\partial u}{\partial x}\frac{\partial^2 v}{\partial x^2} + u\frac{\partial^3 v}{\partial x^3} - v\frac{\partial^3 u}{\partial x^3} + \frac{\partial v}{\partial x}\frac{\partial^2 u}{\partial x^2}\bigg]_b^a = 0. \tag{B.3}$$

Now Equation B.3 leads to the following identity.

$$\int_a^b uL(v) - vL(u)dx = \int_a^b \frac{d}{dx}\bigg(- \frac{\partial u}{\partial x}\frac{\partial^2 v}{\partial x^2} + u\frac{\partial^3 v}{\partial x^3} - v\frac{\partial^3 u}{\partial x^3} + \frac{\partial v}{\partial x}\frac{\partial^2 u}{\partial x^2}\bigg)dx \tag{B.4}$$

$$= \bigg[- \frac{\partial u}{\partial x}\frac{\partial^2 v}{\partial x^2} + u\frac{\partial^3 v}{\partial x^3} - v\frac{\partial^3 u}{\partial x^3} + \frac{\partial v}{\partial x}\frac{\partial^2 u}{\partial x^2}\bigg]_b^a = 0 \tag{B.5}$$

Thus the following holds true and the operator is shown to be self-adjoint.

$$\int_a^b uL(v)dx = \int_b^a vL(u)dx \tag{B.6}$$

□

B.2. Real eigenvalues

In order to determine in which field the eigenvalues are contained, the operator corresponding to the PDE is to be analysed.

For this operator the following theorem holds.

Theorem B.2.1. *For the operator L the eigenvalues, λ, are real valued.*

Proof. The following notation for the real and complex functional inner product is used.

$$\langle \phi, \omega \rangle_{\mathbb{R}} := \int_a^b \phi\omega \ \ dx \ , \langle \phi, \omega \rangle_{\mathbb{C}} := \int_a^b \phi\overline{\omega} \ dx. \tag{B.7}$$

Let ϕ be an eigenfunction of L with eigenvalue λ. Then the following holds true.

$$\langle L(\phi), \phi \rangle_{\mathbb{C}} = \int_a^b L(\phi)\overline{\phi} \ dx = \int_a^b \lambda\phi\overline{\phi} \ dx = \lambda\langle \phi, \phi \rangle_{\mathbb{C}} \tag{B.8}$$

$$\langle \phi, L(\phi) \rangle_{\mathbb{C}} = \overline{\lambda}\langle \phi, \phi \rangle_{\mathbb{C}} \tag{B.9}$$

Now as L is a self-adjoint operator the following holds true.

$$\lambda\langle \phi, \phi \rangle = \langle L(\phi), \phi \rangle = \langle \phi, L(\phi) \rangle = \overline{\lambda}\langle \phi, \phi \rangle. \tag{B.10}$$

Which immediately implies the following.

$$(\lambda - \overline{\lambda})\langle \phi, \phi \rangle = 0 \tag{B.11}$$

Now as $\langle \phi, \phi \rangle \neq 0$, $\lambda = \overline{\lambda}$ and thus $\lambda \in \mathbb{R}$. □

B.3. Non-negative eigenvalues

This section proves the result that the simple homogeneous beam equation has non-negative eigenvalues when subject to physical boundary conditions.

Theorem B.3.1. *The beam equation*

$$EI\frac{\partial^4 u}{\partial x^4} = -\mu\frac{\partial^2 u}{\partial t^2} \tag{B.12}$$

has non-negative eigenvalues λ under physical boundary conditions.

Proof. Using separation of variables the following ODE for the spacial variable is obtained. Denote $u(x,t) = \phi(x)h(t)$.

$$\phi^{(4)} = \lambda\phi \tag{B.13}$$

Using the innerproduct defined in Equation B.7, λ can be expressed in terms of ϕ.

$$\int_a^b \phi^{(4)}\phi dx = \int_a^b \lambda\phi^2 dx \tag{B.14}$$

$$= \left[\phi^{(3)}\phi\right]_a^b - \int_a^b \phi^{(3)}\phi^{(1)} dx \tag{B.15}$$

$$= \left[\phi^{(3)}\phi\right]_a^b - \left[\phi^{(2)}\phi^{(1)}\right]_a^b + \int_a^b \left(\phi^{(2)}\right)^2 dx \tag{B.16}$$

$$= 0 + 0 + \int_a^b \left(\phi^{(2)}\right)^2 dx \tag{B.17}$$

This leads to the following result.

$$\lambda = \frac{\int_a^b \left(\phi^{(2)}\right)^2 dx}{\int_a^b \phi^2 dx} \geq 0 \tag{B.18}$$

□

B.4. Root convergence

Theorem B.4.1. *The positive roots,* y_n*, of* $f(x) = cosh(x)cos(x) + 1$ *and* $n\pi + \frac{\pi}{2}$*, satisfy* $|y_{n+1} - x_{n+1}| < |y_n - x_n|$ *for all* $n \in \mathbb{N}$*.*

Proof. The roots will be shown to converge using a geometrical argument. Note that $\cos(x)$ has roots at $\frac{n\pi}{2}$ for $n \in \mathbb{N}$. Using $f(\frac{n\pi}{2}) = 1$ a triangle can be constructed with $(\frac{n\pi}{2}, 0)$, $(\frac{n\pi}{2}, f(\frac{n\pi}{2}))$ and $(x_0, 0)$ as vertices. By determining x_0 in a clever fashion, the length of the horizontal side of the triangle can be shown to converge to a length of 0. As the root of $f(x)$ sits between $(\frac{n\pi}{2}, 0)$ and $(x_0, 0)$, it must converge to $(\frac{n\pi}{2}, 0)$ as $n \to \infty$.

First the triangle is constructed. As $f(\frac{n\pi}{2}) = 1$, two vertices are already determined. In Figure B.1 the triangle to be formed is shown between the x-axis and the double and dotted line. Now $(x_0, 0)$ is to be determined. To this end the tangent line of $f(x)$ at $\frac{n\pi}{2}$ is used.

The tangent line is of the form $y = ax + b$ for parameters a and b. a is determined using $f'(x)$ at $\frac{n\pi}{2}$. This provides $f'(\frac{n\pi}{2}) = (-1)^{n+1} \cosh(\frac{n\pi}{2}) = a$. Subsequently, b is determined by evaluating the function at $(\frac{n\pi}{2}, 1)$. This simple algebraic task provides $b = 1 + (-1)^n \cosh(\frac{n\pi}{2})$. Now finally x_0 can be determined to be $x_0 = \frac{\frac{n\pi}{2}(-1)^{n+1}}{\cosh(\frac{n\pi}{2})} + \frac{n\pi}{2}$. Then as $n \to \infty$, $d(x_0, \frac{n\pi}{2}) \to 0$.

As such the roots converge and the theorem holds true. □

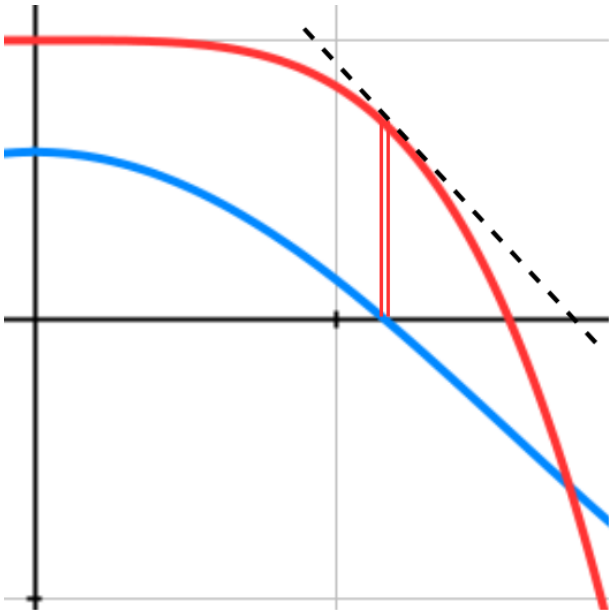

Figure B.1: Triangle formed by the cos, cosh cos, and tangent line of cosh cos.